Modeling contamination migration on the *Chandra X-ray Observatory* — III

Stephen L. O'Dell[*] [a], Douglas A. Swartz [b], Neil W. Tice [c], Paul P. Plucinsky [d], Catherine E. Grant [c], Herman L. Marshall [c], Alexey A. Vikhlinin [d], Allyn F. Tennant [a], and Matthew T. Dahmer [e]

[a] NASA Marshall Space Flight Ctr., MSFC/ZP12, Huntsville, AL 35812, USA
[b] Universities Space Research Assoc., MSFC/ZP12, Huntsville, AL 35812, USA
[c] Massachusetts Institute of Technology, 77 Massachusetts Ave., Cambridge, MA 02139, USA
[d] Smithsonian Astrophysical Observatory, 60 Garden St., Cambridge, MA 02138, USA
[e] Northrop Grumman, MS33, 60 Garden St., Cambridge, MA 02138, USA

ABSTRACT

During its first 16 years of operation, the cold (about -60°C) optical blocking filter of the Advanced CCD Imaging Spectrometer (ACIS), aboard the *Chandra X-ray Observatory*, has accumulated a growing layer of molecular contamination that attenuates low-energy x rays. Over the past few years, the accumulation rate, spatial distribution, and composition have changed. This evolution has motivated further analysis of contamination migration within and near the ACIS cavity, in part to evaluate potential bake-out scenarios intended to reduce the level of contamination.

Keywords: X-ray astronomy, CCDs, contamination, modeling and simulation, spacecraft operations

1. INTRODUCTION

The Advanced CCD Imaging Spectrometer[1] (ACIS, Figure 1) is the most utilized science instrument aboard the *Chandra X-ray Observatory*.[2, 3, 4, 5] Its focal plane comprises a 2×2-CCD imaging array (ACIS-I), which provides sub-arcsecond spectrometric imaging over a 16.9′×16.9′ field, and a 1×6-CCD spectroscopy array (ACIS-S), which reads high-resolution x-ray spectra dispersed by either of *Chandra*'s two objective transmission gratings or serves as a narrow-field spectrometric imager with neither grating inserted. In order to optimize CCD performance, the ACIS focal plane operates at about -120°C, with its detector housing (DH, also called "camera body") normally set at -60°C.

To suppress visible-to-near-infrared light, ACIS-I and ACIS-S each utilize a double-side-aluminized polyimide optical blocking filter[6]—OBF-I and OBF-S—held about 12 mm above the CCD array. Although quite thin—Al/Polyimide/Al = 120/200/40 nm (OBF-I), 100/200/30 nm (OBF-S)—the meshless Luxel™ filters are mechanically robust. The outward face of the OBFs, the camera top, the inner and outer surfaces of the snoot, and the inner surface of the collimator bound the ACIS cavity (Figure 1), which connects to the large Telescope cavity through the Science Instrument Module (SIM) translation table and focus structure. Near the end of the optical bench opposite ACIS, the Telescope cavity vents to space through spacecraft vents and through the aperture of the High-Resolution Mirror Assembly (HRMA). The ACIS cavity, Telescope cavity, and connecting Science Instrument Module (SIM) structure comprise *Chandra*'s Observatory cavity.

The temperature near the edges of the OBFs approach that of the detector housing—i.e., ≈ -60°C—while the centers of the OBFs are somewhat (5°C–20°C) warmer due to radiative heating by the rest of the Observatory cavity. Operating no warmer than -60°C, the ACIS surfaces are by far the coldest surfaces within the Observatory cavity. Based upon the observed attenuation of low-energy x rays[7,8] (§2), these cold surfaces have accumulated a layer (currently, 100–250 μg cm^{-2}) of unidentified molecular contamination[9] over 16 years of operation. Although the accumulation of molecular contamination is 30 times pre-flight estimates, the total mass of condensed contaminant(s) is calculated to be < 1 g.

[*] Contact author (SLO): stephen.l.odell@nasa.gov; voice +1 (256) 961-7776; fax +1 (256) 961-7522
Postal address: NASA/MSFC/ZP12; 320 Sparkman Drive NW; Huntsville, AL 35805-1912, USA

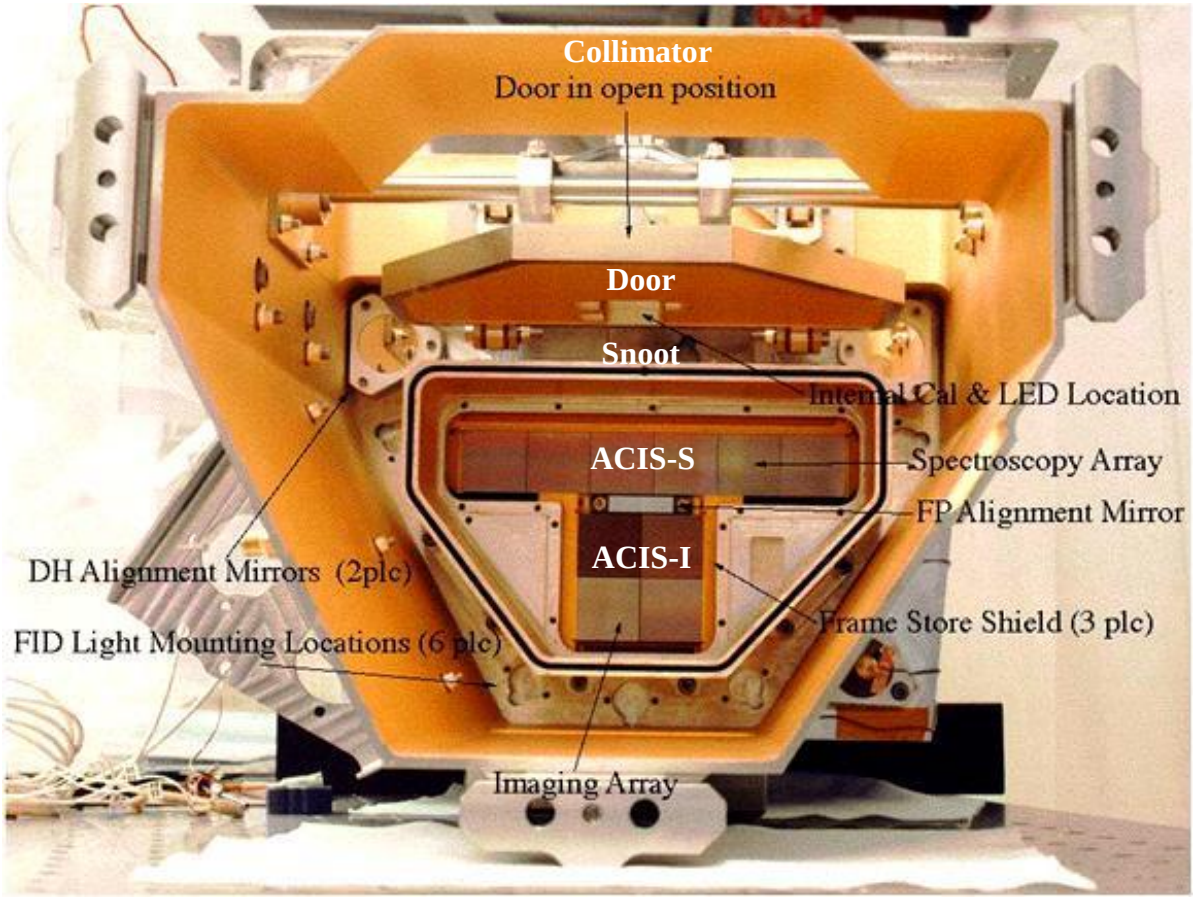

Figure 1. Top view of the engineering unit of *Chandra*'s Advanced CCD Imaging Spectrometer (ACIS), showing the 2×2-CCD ACIS-I and the 1×6-CCD ACIS-S focal planes. In the flight unit, aluminized-polyimide optical blocking filters OBF-I and OBF-S cover, respectively, the I and the S arrays. The OBFs reside within the "snoot" (with the door sealed closed until *Chandra*'s on-orbit check-out), which in turn lies within the ACIS "collimator".

In order to simulate accumulation of molecular contamination on the OBFs and to assess potential mitigation scenarios—e.g., bake-outs—we developed the *Chandra* contamination-migration model (CCMM). Using methods analogous to those used for radiative transport in the thermal analysis and essentially the same geometric model for the Observatory cavity, the CCMM simulates molecular transport of a contaminant amongst the surfaces in the Observatory cavity, including sources and sinks (vents).

Paper I[10] of this series described the CCMM, which then (2004) used a rather low-resolution geometric model of the *Chandra* Observatory cavity. CCMM simulations supported a detailed study[11] by the *Chandra* Team to evaluate risks, benefits, and efficacy of baking ACIS to eliminate or at least reduce molecular contamination accumulated on the OBFs. The Team's comprehensive investigation found that a room-temperature bake-out, which had been anticipated in the instrument's design and used once early in the mission, did not pose a credible risk either to the ACIS or to the spacecraft. However, without definitive constraints on the volatility of the contaminant, the CCMM simulations showed that the parameter space for a successful bake-out was not large and that a bake-out might result in more contamination on the OBFs. For this reason and because the rate of accumulation was slowing, the *Chandra* Team postponed indefinitely a decision on baking the ACIS.

The accumulation rate of molecular contamination continued to decline until about 2010, when it began to rise. This prompted a renewed interest in the molecular-transport simulations. Paper II[12] (2013) described the revised CCMM, which

used a higher-resolution geometric model of the ACIS cavity—albeit lower-resolution for the rest of the *Chandra* cavity—and a thermal model developed with modern finite-element tools. The motivation for the higher-resolution model for the ACIS cavity was to provide a high-fidelity geometric and thermal model for surfaces with strong temperature gradients—namely, the OBFs and the collimator.

This current paper (III) extends the study reported in Paper II, using the same geometric, thermal, and contamination-migration models. The evolution of the accumulation rate and spatial distribution of molecular contamination on the OBFs, along with potential relationships with temperature changes within the *Chandra* Observatory cavity, provide some constraints on the volatility of at least one contaminant on the OBF. Furthermore, due to the continuing increase in the accumulation rate, the *Chandra* Team will revisit the issue of a bake-out over the next year or so. Hence, this paper reports initial steps in using the CCMM to support the new bake-out study. Section 2 reports the current status of the molecular contamination on the OBF. Section 3 reviews the geometric, thermal, and molecular-transport model of the ACIS cavity. Next, Section 4 reports preliminary results of example bake-out simulations using the CCMM. Finally, Section 0 summarizes the findings of this continuing investigation to date.

2. MOLECULAR CONTAMINATION ON ACIS FILTERS

In this section, we give an update on the observed evolution of molecular contamination on the ACIS OBF (§2.1). We also note changes in the thermal state of the Observatory that *might* alter the accumulation rate and gradient (§2.2). Such a correlation would be important in potentially constraining the volatility of the accumulated contaminant(s).

2.1. Observed evolution

As described in Papers I and II, various ACIS spectrometric and LETG/ACIS-S high-resolution spectroscopic observations measure x-ray absorption by contamination accumulated on the ACIS OBFs. Figure 2 documents the evolution of the mass column of C, O, and F on OBF-S, based upon fits of their absorption edges to LETG/ACIS-S high-resolution spectroscopy of cosmic x-ray sources. The left panel shows the accumulation of these contaminant elements from the start of 2000 to mid 2015, at 2 (or 3) distances from the CCD edge nearest the OBF frame. The right panel displays the accumulation *rate* of C and of O over the same time span. Although this plot is just the time derivative of the plot to the left, it perhaps illustrates more clearly the temporal evolution: The accumulation rate decreased from the beginning of science operations until around 2010, when it began increasing again. The right panel of Figure 2 also suggests a change in the composition of the accumulating molecular contamination: Most evident is the apparently very small rate of accumulation of oxygen-bearing contamination during 2004–2008.

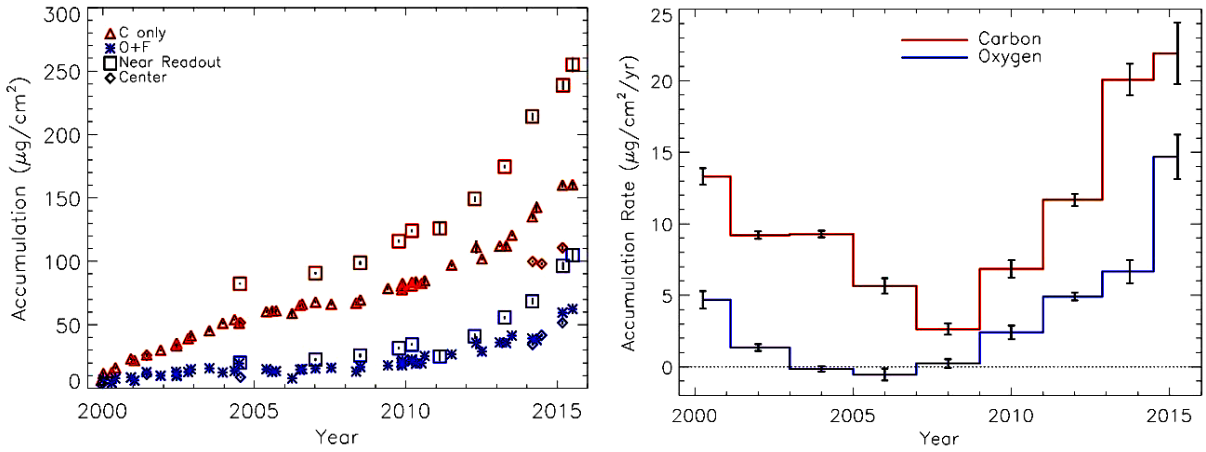

Figure 2. Evolution of the mass column of molecular contamination on the ACIS optical blocking filter (OBF), as determined from high-resolution spectra obtained using *Chandra*'s Low-Energy Transmission Gratings with ACIS-S (LETG/ACIS-S). Left panel shows the accumulated mass column of carbon (red markers) and of oxygen and fluorine (blue markers) for CCD rows near the ACIS-S edge (squares), for rows about a third of the way toward the middle (triangles for C, × for O and F), and for rows near the middle (diamonds for C only). Right panel displays the accumulation *rate* of carbon (upper, red line) and of oxygen (lower, blue line) for rows about a third of the way toward the ACIS-S middle.

2.2. Possible relation to temperature changes

If the thermal state is constant in time, contamination sources eventually deplete and the deposition rate declines while the vaporization rate (a sensitive function of temperature) remains constant. This naturally accounts for the early decrease in the accumulation rate onto the OBFs. As the accumulation rate onto a surface equals the deposition rate minus the vaporization rate, the increasing accumulation rate after 2010 (§2.1) indicates faster deposition or slower vaporization. Each of these may result from temporal changes in the thermal state: Decreasing OBF temperatures slow vaporization of contamination from the OBF surface, while increasing temperatures in other areas of the Observatory cavity could increase outgassing rates, thus effecting faster deposition of contamination onto the OBF surface. Figure 3 documents changes in the thermal state that are possibly relevant to the increasing rate of contamination accumulation onto the OBF, which started around 2010.

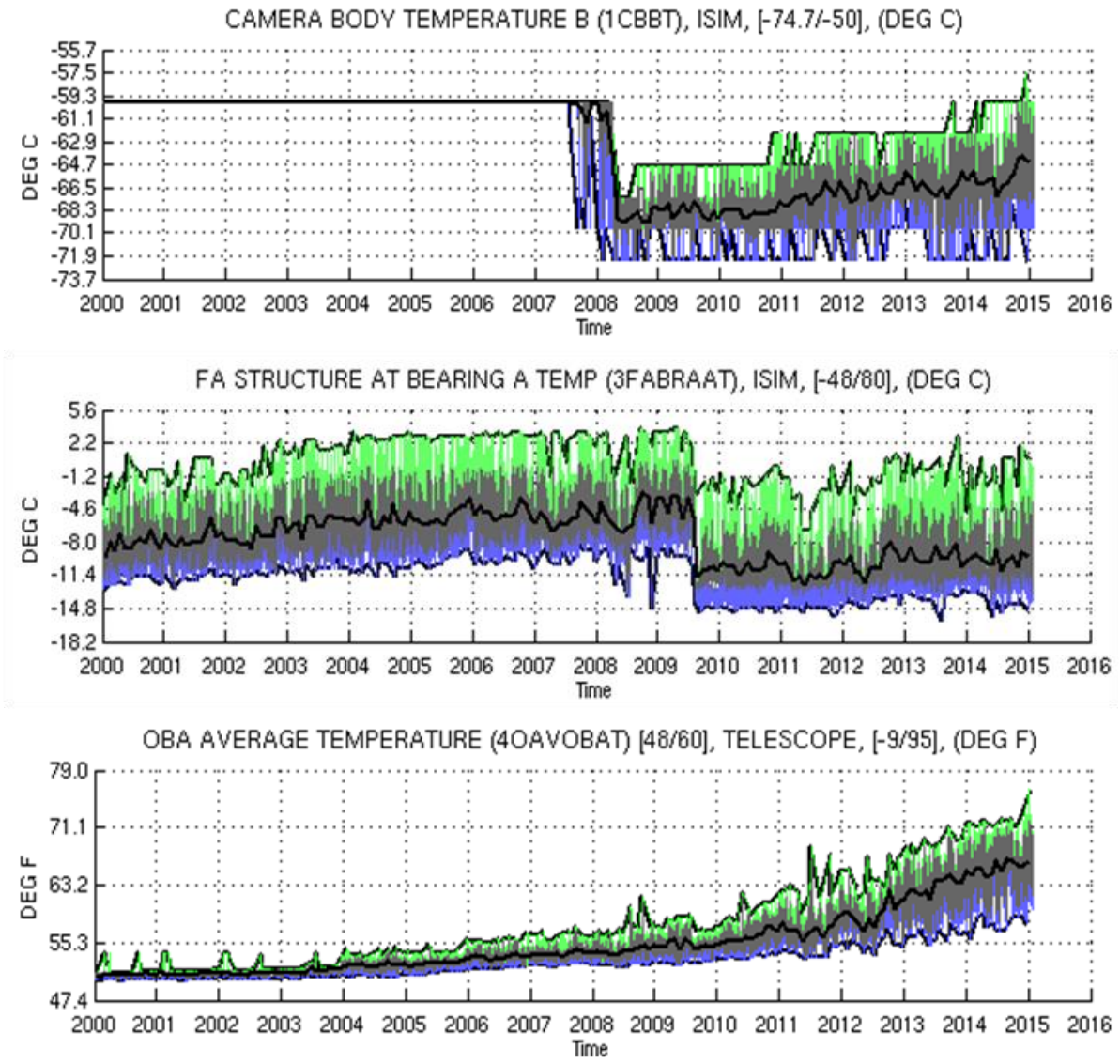

Figure 3. Recorded temperatures of the ACIS camera body (top panel), of the SIM focus structure (middle panel), and of the Optical Bench Assembly (bottom panel). Heaters held the camera body at a constant temperature until they were turned OFF in 2008 April, in order to help keep the focal-plane temperature near -120°C.

Turning OFF the ACIS detector-housing heater in 2008 April immediately lowered the temperature (Figure 3 top panel) of the ACIS camera top and OBF frames (and, hence, OBF edges) by about 8°C—approximately from -61°C to -69°C. As Figure 4 illustrates, an 8°C drop in temperature near -60°C dramatically lowers the vaporization rate—by a factor of 10–30. Thus, if the vaporization rate of a contaminant were initially comparable to the deposition rate, lowering the temperature would lower the vaporization rate and thus increase the accumulation rate. As a test of the influence of the ACIS detector-housing heater upon the accumulation rate near the edges of the OBF, this heater was returned to the ON state during 2015 August 11. It is still too early to assess to what degree this change in the thermal state is affecting the contamination accumulation rate near the OBF boundaries.

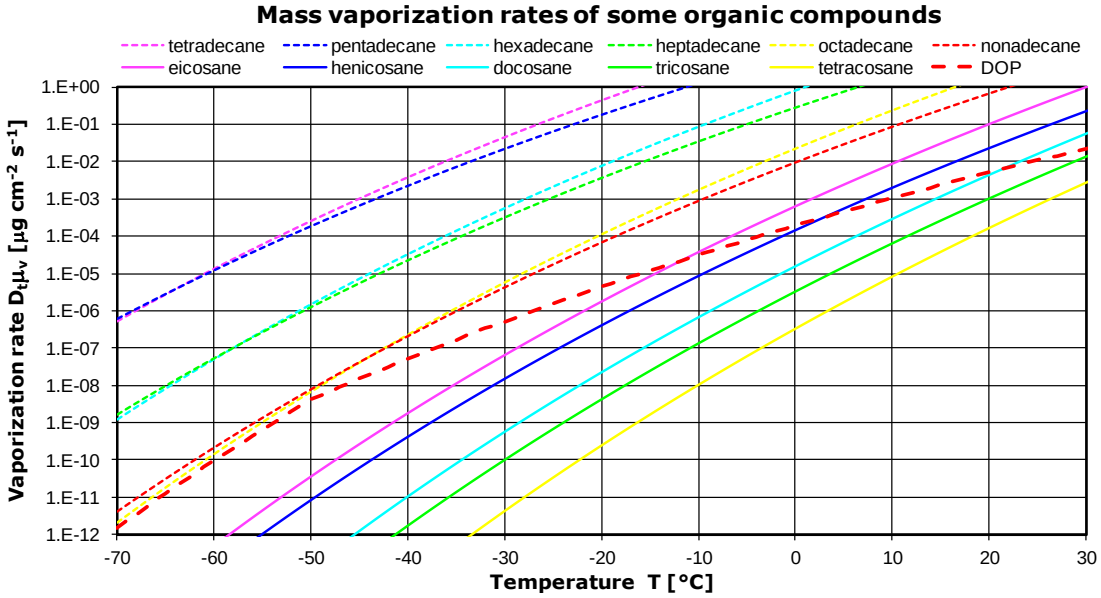

Figure 4. Temperature dependence of the mass vaporization rate of several simple organic compounds. Note the strong dependence upon temperature, which is related to the vaporization enthalpy of the compound[13].

The alternative to decreased vaporization is increased deposition, as would occur if a new source of contamination appears or if an existing source elsewhere in the Observatory cavity outgasses more rapidly due to rising temperatures within the Observatory Unfortunately, rising temperatures within the Observatory—e.g., the warming of the optical bench assembly (OBA) by about 10°C (Figure 3 bottom panel)—make it plausible that the source rate for release of molecular contamination within the Observatory cavity may be increasing.

3. MODELS FOR ACIS CAVITY

In this section, we briefly review the models and methodology for simulating molecular transport within the Observatory cavity, which Paper II[12] describes in more detail. The simulations use a geometric model (§3.1) combined with thermal boundary conditions to construct a thermal model (§3.2) of the temperature distribution within the Observatory cavity. Given the geometric model, the thermal model's surface temperatures, the molecular-volatility properties, and other boundary conditions—including external contamination sources and sinks (vents)—the contamination-migration model (§3.3) governs molecular transport within the Observatory cavity for specific assumptions and scenarios (§3.3).

3.1. Geometric model

Figure 5 displays the geometric model developed in Paper II[12] and employed in the current study. The external view (left panel) illustrates the simplified treatment of the Telescope cavity and of the SIM conduit to the ACIS cavity, which we reduced to a Telescope Closeout and Translation-table Closeout, respectively. The internal view (right panel) shows the more detailed treatment of the ACIS cavity, which provides higher resolution for surfaces of interest (especially the OBFs) and includes potentially important features near the OBF surfaces.

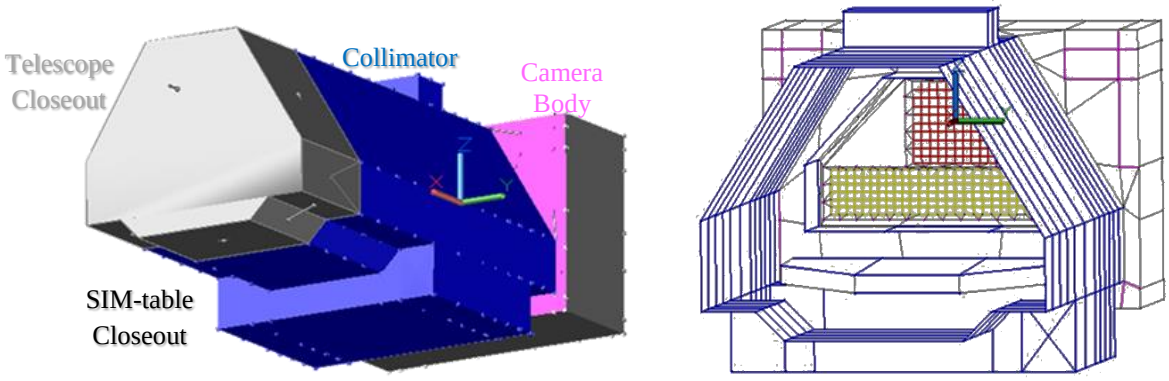

Figure 5. Geometric model for the *Chandra* Observatory cavity, used for the thermal analysis and for the molecular-transport analysis in the current study. The external view (left panel) illustrates the simplified treatment of the geometry outside the ACIS cavity; the interior view (right panel) displays the more complex treatment of the geometry within the ACIS cavity, especially for the optical blocking filters OBF-I (red square grid) and OBF-S (yellow rectangular grid).

The geometric model gives the area A_j of each surface element j and the matrix f_{jk} of geometric view factors (Figure 6). As the view factor specifies the fraction of the flux from one surface impingent upon a second surface, it is an essential geometric attribute in any transport analysis—either radiative or molecular.

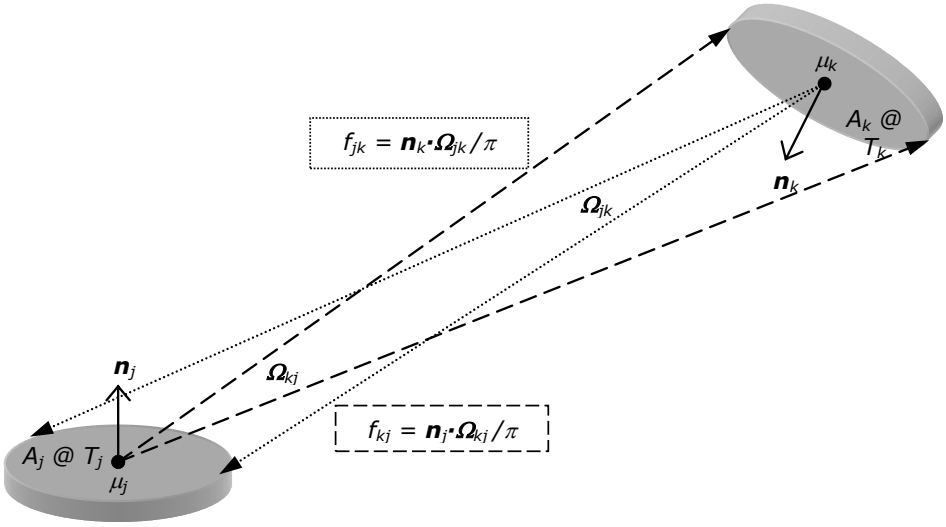

Figure 6. Drawing identifying the geometric "view factor", used to analyses radiative or molecular transport amongst surfaces.

3.2. Thermal model

Besides the geometric model, thermal analysis requires specification of the radiative emissivity ε_j for each surface element, conductive linkages amongst elements, and the thermal boundary conditions. Most of the ACIS cavity is conductively coupled; however, the OBF away from its edges is predominantly radiatively coupled to the rest of the Observatory cavity. Temperatures of the conductively coupled surface elements are generally well determined using telemetry from numerous onboard temperature sensors.

In contrast, temperatures of surface elements of predominantly radiatively coupled components—most importantly the OBFs—are significantly less certain. Based upon temperatures within the Telescope cavity, we set the radiative sink at the Telescope Closeout (Figure 5 left panel) to +18°C when ACIS is in the observing position or to a telemetered boundary temperature when it is stowed. The largest uncertainty in modeling the temperature distribution on the OBFs results from uncertainty in its radiative emissivity ε_j: While the emissivity of the pristine surface is about 0.05, the emissivity of the

contaminated surface is substantially larger. For the thermal modeling presented here, we set the radiative emissivity of contaminated surfaces—most importantly the outward OBF surface (facing the Observatory cavity)—to 0.4 and assume that the inward OBF surface (facing the focal plane at -120°C) has remained pristine. Figure 7 and Figure 8 exhibit the temperature distribution within the ACIS cavity for four relevant thermal states.

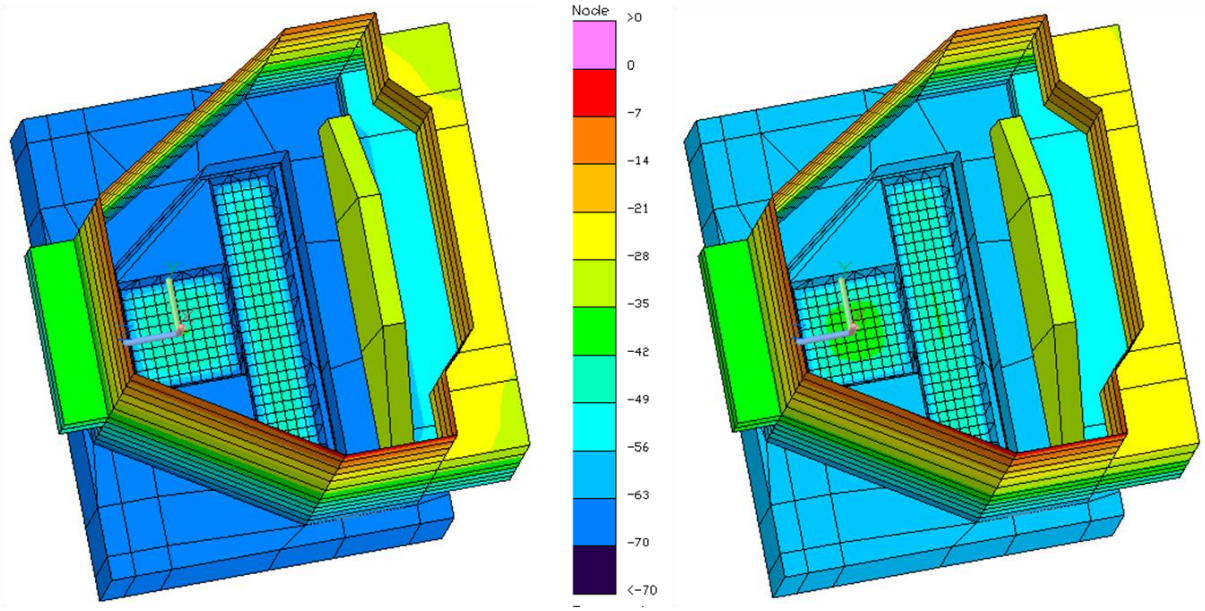

Figure 7. Temperature distribution over the ACIS instrument, during operation with the detector-housing heater OFF (left panel) or with it ON (right panel). With the heater ON, the temperature of the camera body and, hence, OBF frames is regulated at about -60°C; with the heater OFF, that temperature floats around -66°C (with current thermal loads). In either case, the operational temperature of the CCD focal plane is set to -120°C.

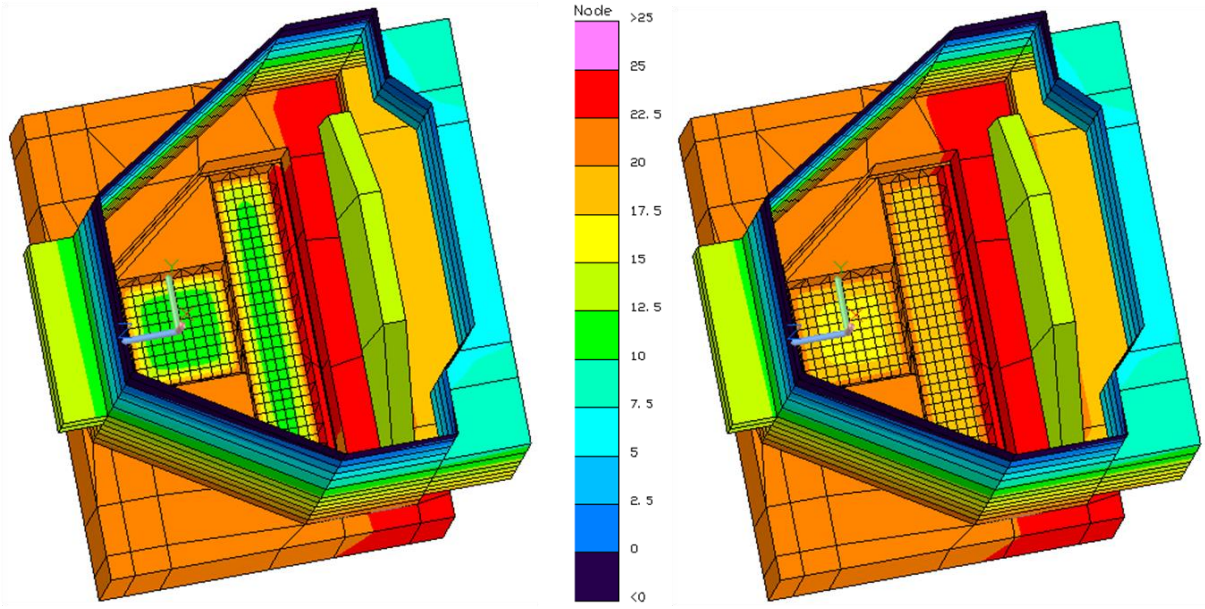

Figure 8. Temperature distribution over the ACIS instrument, during two potential bake-out scenarios. For a cool-focal-plane bake-out (left panel), the focal-plane temperature is set to -60°C; for a warm-focal-plane bake-out (right panel), it is set to +25°C. In either case, the detector-housing temperature is set to +25°C.

3.3. Molecular-transport model

The calculation of molecular transport is quite similar to the calculation of radiative transport in the thermal model (§3.2). Here we employ the methodology used in our previous studies of contamination migration (Papers I and II). For each surface element *j*, The molecular-transport model requires as input the area A_j and view factor f_{jk} to all other elements k, determined using the geometric model (§3.1); the temperature T_j for each surface element *j*, established using the thermal model and boundary conditions (§3.2); and information on the temperature-dependent volatility of the contaminant—e.g., the mass-column vaporization rate $\dot{\mu}_v(T)$ of the contaminant.

The transport equation calculates the evolution of the mass column μ_j of the contaminant on each surface element *j*, where the accumulation rate onto surface *j* is simply the deposition rate due to vaporization from all other surfaces *k* onto *j* (and to external sources), minus the vaporization rate from surface *j*:

$$\frac{d\mu_j}{dt} = +\left\{\sum_k \dot{\mu}_v(T_k)\Theta(\mu_k)\, f_{jk}\, \frac{A_k}{A_j}\right\} - \left\{\dot{\mu}_v(T_j)\Theta(\mu_j)\right\},$$

where the unit step distribution $\Theta(\mu)$ enforces the physical condition that the mass column cannot be negative. As boundary conditions on the exchange of material between the ACIS cavity and the rest of the Observatory cavity, we treat the Telescope Closeout as a source and sink.

The rate of vaporization—evaporation or sublimation, as appropriate to the phase of the deposited species—is simply related to the vapor pressure $P_v(T)$ through

$$\dot{\mu}_v(T) = \frac{P_v(T)}{\sqrt{2\pi\, RT/M}},$$

with *R* the ideal gas constant and *M* the molar mass of the contaminant. To obtain the temperature dependence of the mass vaporization rate, we use the Clausius–Clapeyron relation for $P_v(T)$ to obtain $\dot{\mu}_v(T)$ at temperature *T* as a function of its value at a reference temperature T_o:

$$\dot{\mu}_v(T) = \dot{\mu}_v(T_\circ)\sqrt{\frac{T_\circ}{T}}\, \exp\left[-\frac{\Delta_v H}{R}\left(\frac{1}{T} - \frac{1}{T_\circ}\right)\right],$$

where the vaporization (evaporation or sublimation, as appropriate) enthalpy $\Delta_v H$ governs the temperature sensitivity. Figure 4 uses the above equations to plot the vaporization rate $\dot{\mu}_v(T)$ for several simple organic compounds, using tabulated values[13] for $P_v(T_\circ)$ and for $\Delta_v H$.

Before showing the results of some example CCMM simulations, we mention some underlying assumptions and approximations in the molecular-transport model. First, we assume that molecules move ballistically from one surface to another, which is true for the long collisional mean-free-path at the low pressures relevant to the simulation. Second, we neglect surface migration, which plausibly plays a role—especially for a material that is liquid at relevant temperatures. Furthermore, if there is more than one species of contaminant, we treat the migration of each independently.

4. EXAMPLE SIMULATIONS

We have run several CCMM simulations using the models described above. The main obstacle to obtaining definitive answers from the simulations is the uncertainty in the volatility of the contaminant(s). However, changes in the thermal state of the Observatory cavity and in the accumulation rate and spatial distribution are placing some constraints on the volatility. Figure 9 exhibits results of contamination-migration simulations, under identical thermal conditions, for a contaminant of relatively low volatility (left panel) and for one of relatively moderate volatility (right panel). For relatively low volatility (left panel), the accumulation is deposition-dominated and slightly peaked near the OBF's center, due to geometric concentration and shadowing effects in the deposition. For relatively moderate volatility (right panel), the

vaporization rate on the warmer parts of the OBF is comparable to the deposition rate, resulting in less accumulation near the (warmer) center of the respective OBF than near its (cooler) edge. For high volatility (not shown), vaporization dominates deposition and the OBF cleans, starting from the (warmer) center outward to the (cooler) frame.

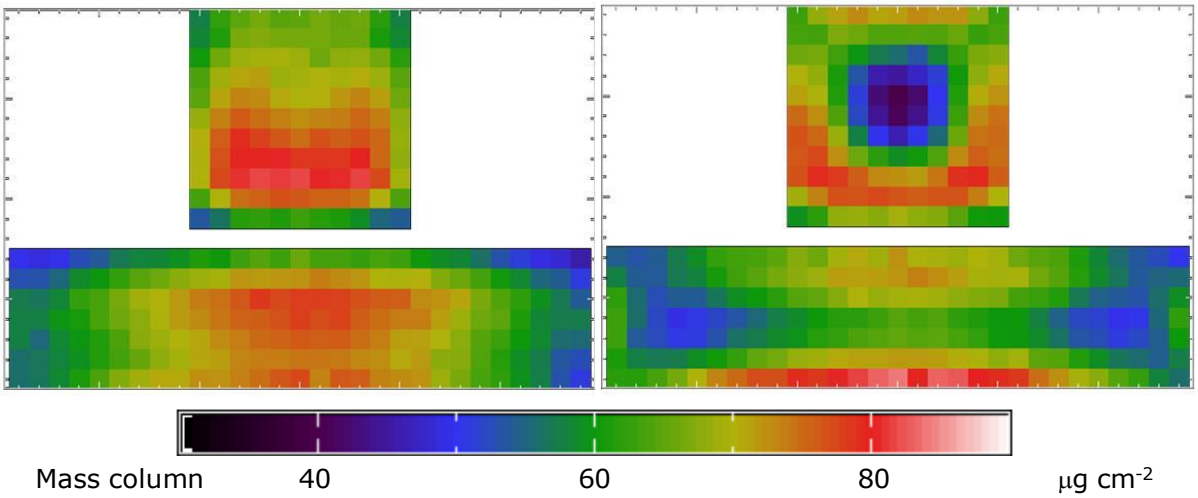

Figure 9. Distribution of mass column of accumulated contamination on the ACIS OBFs, based upon molecular-transport simulations for a contaminant of relatively low volatility (left panel) and for one of relatively moderate volatility (right panel).

That the distribution of contamination on the ACIS OBFs is thickest near the OBF edges suggests that the volatility of at least one contaminant species is such that vaporization is competitive with deposition over warmer areas of the OBFs. This engenders some optimism that it may be possible to devise a bake-out procedure to achieve at least partial cleaning of the OBFs. However, the evolution (§2.1) of accumulated mass column (Figure 2 left panel) and composition (Figure 2 right panel) indicates that at least two components are present. Figure 10 displays results of a CCMM simulation of the accumulation of contamination comprising two (independent) components—a contaminant of moderately low volatility with a source rate dropping exponentially on a 3.7-year timescale due to depletion; and a contaminant of somewhat higher volatility with a source rate rising exponentially with the increasing temperature of the optical bench. Results such as these provide initial conditions—mass column on each surface element—for a CCMM simulation of a bake-out.

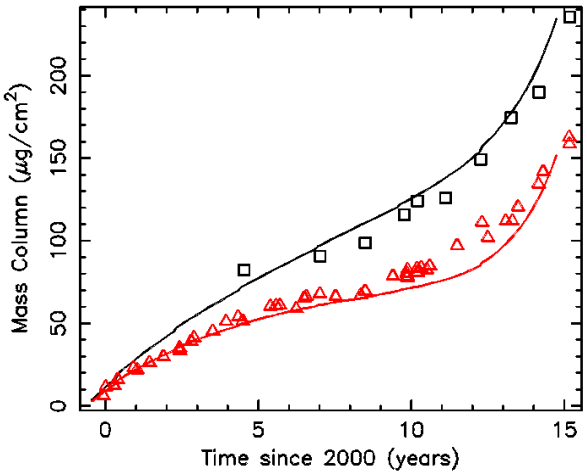

Figure 10. Molecular-transport simulations for accumulation of two-component contamination on the ACIS OBF-S compared to the mass-column evolution measured with the LETG/ACIS-S (Figure 2). The black line and square markers denote the model and data for rows near the ACIS-S edge; the red line and triangle markers, for rows about one-third toward the middle.

To demonstrate the bake-out simulation, we present some example cases. As we have not identified the contaminant(s) on the ACIS OBFs, we use dioctyl phthalate (DOP) as a reference molecule. DOP ($C_{24}H_{38}O_4$)—also known as diethylhexyl phthalate (DEHP)—is a plasticizer implicated in contamination of CCDs on other x-ray missions.[14,15] LETG/ACIS-S observations of the spectral signature of the contamination on the *Chandra* OBFs are consistent with DOP being a significant (but not sole) component of the lower-volatility contaminants accumulated over the first 5–10 years of the mission. However, such observations indicate that the dominant contaminant accumulating more recently is much too oxygen-rich (C/O≈1) to be DOP (C/O=6). The volatility of DOP is also in the range of interest for contamination of the ACIS OBFs during the first decade of operation, while the dominant component of the more recent contamination appears to have a slightly higher volatility.

Figure 11 exhibits results of CCMM simulations of DOP transport under two room-temperature bake-out scenarios—warm focal plane (left panels) and cool focal plane (right panels). As one would expect, the OBF clears much faster with a warm (+25°C) focal plane than with a cool (-60°C) one. On the other hand, the temperature of the focal plane has little influence on the long time required to vent the Observatory to space. The cool temperatures (≈ -10°C) of the SIM structure and the upper zones of the ACIS collimator throttle down the flow from the ACIS cavity into the Telescope cavity.

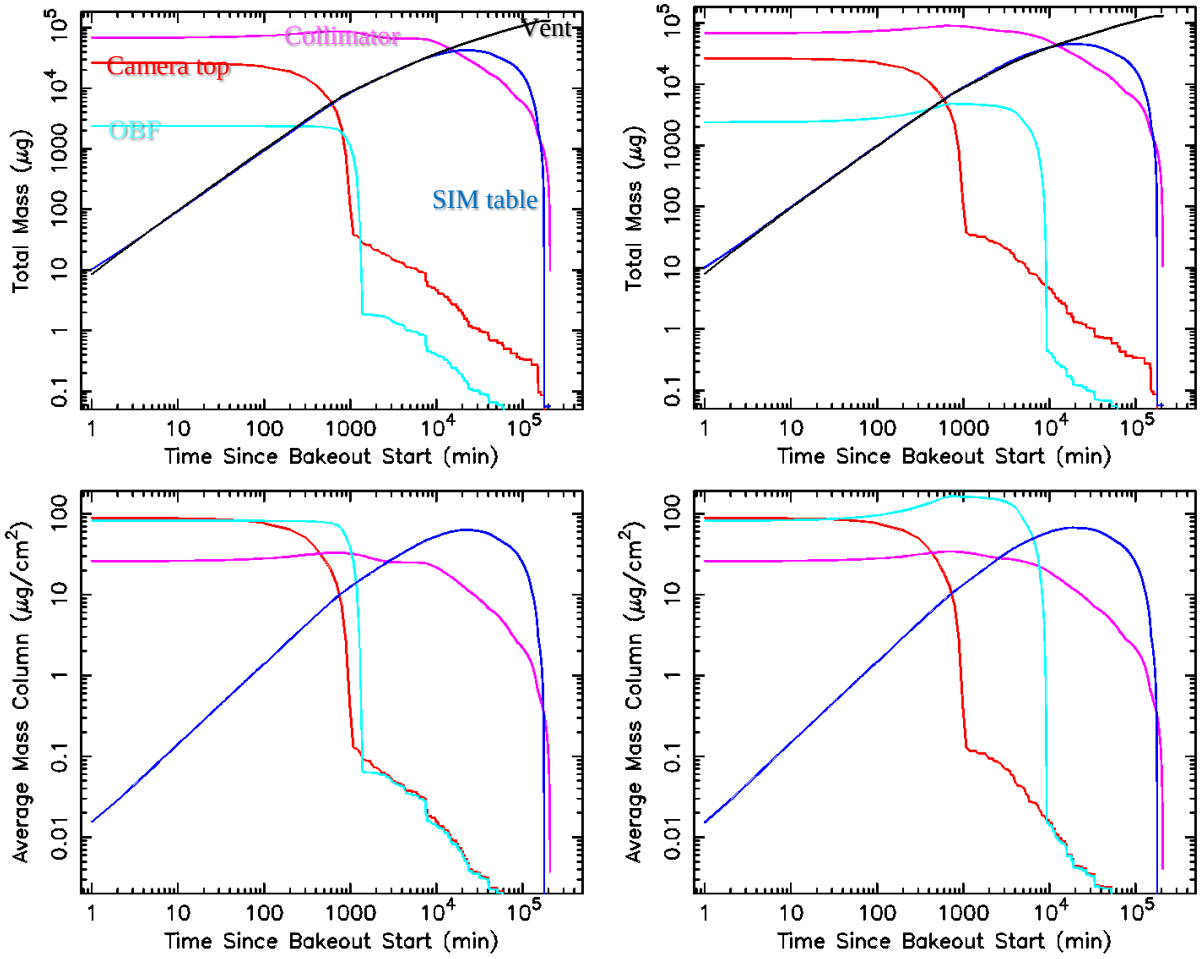

Figure 11. CCMM simulations for an ACIS room-temperature bake-out of an example molecular contaminant—the plasticizer dioctyl phthalate (DOP) or diethyhexyl phthalate (DEHP). Left panels show results for a warm (+25°C) focal plane; right panels, for a cool (-60°C) focal plane. Upper panels plot the total contaminant mass on each component; lower panels, the average mass column on each component.

The slow response of DOP at warm temperatures results from its low melting point (-50°C) compared to other molecular contaminants having a similar volatility at colder temperatures (< -50°C). As the enthalpy of sublimation is significantly less than the enthalpy of evaporation, the temperature dependence of the mass vaporization is markedly weaker for a liquid (see Figure 4). For comparison, we perform the same bake-out simulations for octadecane de-rated to 60% of its vaporization rate, to match the mass vaporization rate of DOP below -50°C (Figure 4).

Figure 12 exhibits results of CCMM simulations of (de-rated) octadecane transport under two room-temperature bake-out scenarios—warm focal plane (left panels) and cool focal plane (right panels). As one would expect, the OBF clears faster with a warm (+25°C) focal plane than with a cool (-60°C) one, although the timescale is short in either case. Again, the temperature of the focal plane has little influence on the time required to vent the Observatory to space. However, for octadecane, the venting timescale is only a few days—compared to a few months for DOP.

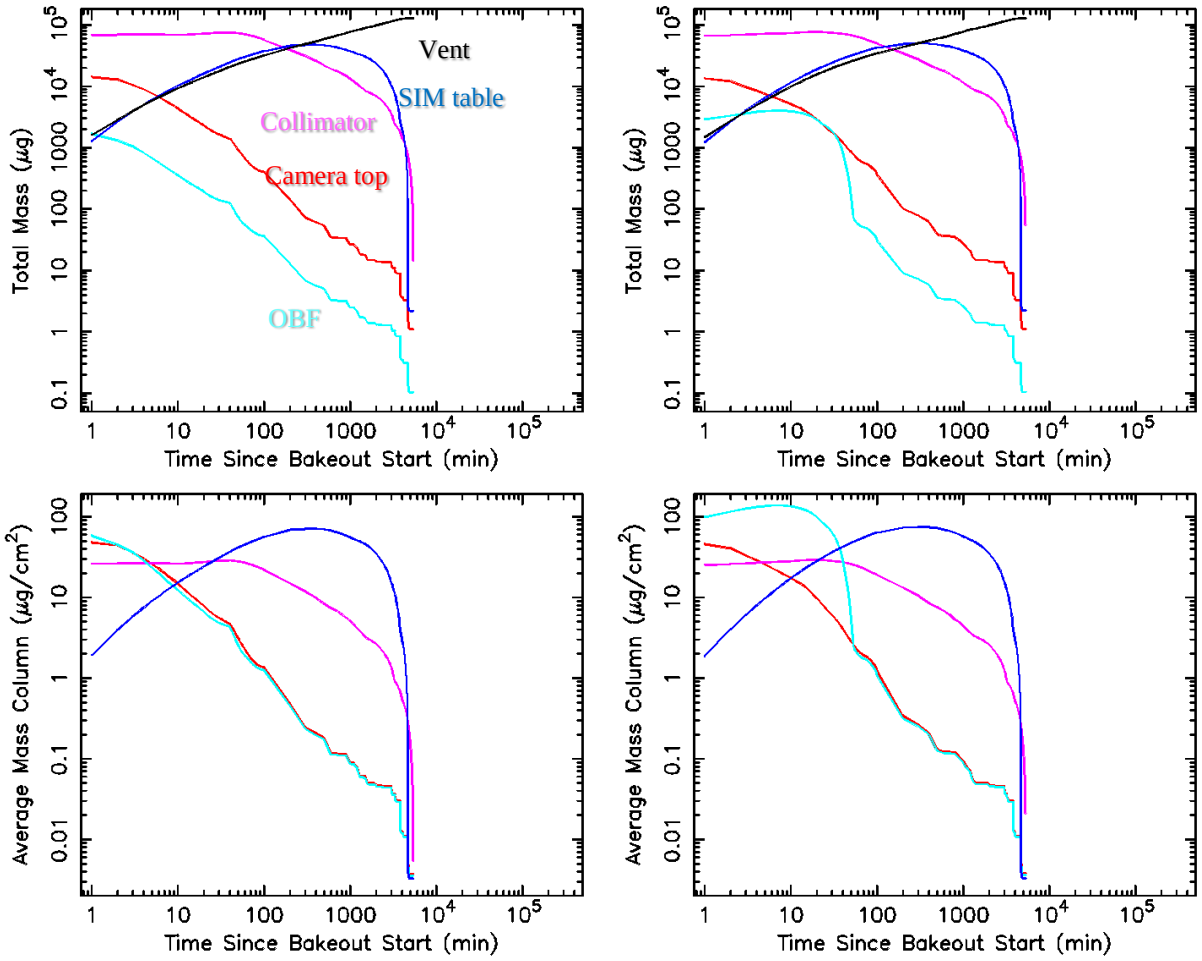

Figure 12. CCMM simulations for an ACIS room-temperature bake-out of an example molecular contaminant—octadecane, slightly de-rated to match the volatility of DOP at low temperatures (see text). Left panels show results for a warm (+25°C) focal plane; right panels, for a cool (-60°C) focal plane. Upper panels plot the total contaminant mass on each component; lower panels, the average mass column on each component.

5. SUMMARY

Although we are hopeful about cleaning the OBFs (at least partially), there are clearly uncertainties in the modeling. We are comfortable with the fidelity and accuracy of the geometric model of the ACIS cavity (§3.1) and with most of the thermal model (§3.2), which is largely conductively coupled and utilizes onboard temperature measurements. However, the evident role of the SIM structure in governing the venting to space during a bake-out, requires a higher-fidelity geometric and thermal model of this part of the Observatory cavity. Unfortunately, the largest uncertainty in the thermal modeling is the temperature distribution on the contaminated OBFs. As the OBFs are predominantly radiatively coupled, their temperature distribution is sensitive to the emissivity ε of their surfaces (§3.2), which in turn depends upon the thickness and properties of the contaminant(s) on its surfaces.

Of course, the largest uncertainty follows from lack of identification of the molecular contaminant(s). Comparing simulation results with the observed evolution of the mass column and changes in the thermal state of the Observatory helps constrain the properties of the contaminant(s), thus providing some confidence in simulation results for potential bake-out scenarios. However, the possibility of a phase transition between operating temperatures and bake-out temperatures means that knowledge of a contaminant's volatility at operating temperatures does not necessarily adequately constrain its volatility at bake-out temperatures—cf. Figure 11 (DOP) and Figure 12 (octadecane).

Finally, the contamination-migration modeling neglects some complicating physical effects that may be important. One of these is surface migration, which may play a role in transport on the OBF surface—especially for a liquid similar to dioctyl phthalate (DOP). Another complication is the physical interaction of multiple contaminants in the condensed state: The simulations treat each contaminant species independently, whereas one might overlie another or be mixed together.

ACKNOWLEDGEMENTS

The *Chandra X-ray Observatory* is operated by the Smithsonian Astrophysical Observatory (SAO) under contract to NASA Marshall Space Flight Center (MSFC). The Advanced CCD Imaging Spectrometer (ACIS) was developed by the Massachusetts Institute of Technology (MIT) and Pennsylvania State University.

REFERENCES

[1] Garmire, G. P., Bautz, M. W., Ford, P. G., Nousek, J. A., & Ricker, G. R., Jr., "Advanced CCD Imaging Spectrometer (ACIS) instrument on the Chandra X-ray Observatory", SPIE 4851, 28–44 (2003).

[2] Weisskopf, M. C., "The Chandra X-Ray Observatory: progress report and highlights", SPIE 8443, 0Y 9pp (2012).

[3] Weisskopf, M. C, Aldcroft, T. L., Bautz, M., Cameron, R. A., Dewey, D., Drake, J. J., Grant, C. E., Marshall, H. L., & Murray, S. S., "An overview of the performance of the Chandra X-ray Observatory", Exp. Astron. 16, 1–68 (2003).

[4] Weisskopf, M. C., Brinkman, B., Canizares, C., Garmire, G., Murray, S., & Van Speybroeck, L. P., "An overview of the performance and scientific results from the Chandra X-ray Observatory", Pub. Astron. Soc. Pacific 114, 1–24 (2002).

[5] Weisskopf, M. C., Tananbaum, H. D., Van Speybroeck, L. P., & O'Dell, S. L., "Chandra X-ray Observatory (CXO): overview", SPIE 4012, 2–16 (2000).

[6] Powell, F. R., Keski-Kuha, R. A., Zombeck, M. V., Goddard, R. E., Chartas, G., Townsley, L. K., Moebius, E., Davis, J. M., & Mason, G. M., "Metalized polyimide filters for x-ray astronomy and other applications", SPIE 3113, 432–440 (1997).

[7] Plucinsky, P. P., Schulz, N. S., Marshall, H. L., Grant, C. E., Chartas, G., Sanwal, D., Teter, M., Vikhlinin, A. A., Edgar, R. J., Wise, M. W., Allen, G. E., Virani, S. N., DePasquale, J. M., & Raley, M. T., "Flight spectral response of the ACIS instrument", SPIE 4851, 89–100 (2003).

[8] DePasquale, J. M., Plucinsky, P. P., Vikhlinin, A. A., Marshall, H. L., Schulz, N. S., & Edgar, R. J., "Verifying the ACIS contamination model with 1E0102.2-7219", SPIE 5501, 328-338 (2004).

[9] Marshall, H. L., Tennant, A., Grant, C. E., Hitchcock, A. P., O'Dell, S. L., & Plucinsky, P. P., "Composition of the Chandra ACIS contaminant", SPIE 5165, 497–508 (2004).

[10] O'Dell, S. L., Swartz, D. A., Plucinsky, P. P., Freeman, M. A., Markevitch, M. L., Vikhlinin, A. A., Chen, K. C., Giordano, R. J., Knollenberg, P. J., Morris, P. A., Tran, H., Tice, N. W., & Anderson, S. K., "Modeling contamination migration on the Chandra X-ray Observatory", SPIE 5898, 313–324 (2005). [Paper I]

[11] Plucinsky, P. P., O'Dell, S. L., Tice, N. W., Swartz, D. A., Bautz, M. W., DePasquale, J. M., Edgar, R. J., Garmire, G. P., Giordano, R., Grant, C. E., Knollenberg, P., Kissel, S., LaMarr, B., Logan, R., Mach, M., Marshall, H. L., McKendrick, L., Prigozhin, G. Y., Schwartz, D., Schulz, N. S., Shropshire, D., Trinh, T., Vikhlinin, A. A., & Virani, S. N., "An evaluation of a bake-out of the ACIS instrument on the Chandra X-Ray Observatory", SPIE 5488, 251–263 (2004).

[12] O'Dell, S. L., Swartz, D. A., Tice, N. W., Plucinsky, P. P., Grant, C. E., Marshall, H. L., Vikhlinin, A., & Tennant, A. F., "Modeling contamination migration on the Chandra X-ray Observatory II", SPIE 8859, 0F 12pp (2013). [Paper II]

[13] Acree, W., Jr., & Chickos, J. S., "Phase transition enthalpy measurements of organic and organometallic compounds. Sublimation, vaporization, and fusion enthalpies from 1880 to 2010", J. Phys. Chem. Ref. Data 39, 043101 942pp (2010).

[14] Mori, H., Tsuru, T. G., Matsumoto, H., Uchiyama, H., Ozawa, M., Takikawa, Y., Nobukawa, M., Koyama, K., Torii, K., Tawa, N., Kitamoto, S., Sudoh, K., & Kohmura, T., "Ground bakeout experiment of the optical blocking filter (OBF) for the Suzaku XIS", SPIE 6686, 0O 12pp (2007).

[15] Urayama, F., Bando, T., Kano, R., Hara, H., Narukage, N., & Sakao, T., "Molecular contamination assessments on Hinode X-Ray Telescope", JSASS 56, 536-542 (2008).